BNL-64648



ConF-970526--

# The E2/M1 Ratio in Δ Photoproduction

A.M. Sandorfi[1], G. Blanpied[4], M. Blecher[6], A. Caracappa[1], C. Djalali[4], G. Giordano[2], K. Hicks[7], S. Hoblit[1,5], M. Khandaker[6,1], O.C. Kistner[1], A. Kuczewski[1], M. Lowry[1], M. Lucas[4], G. Matone[2], L. Miceli[1,4], B. Preedom[4], D. Rebreyend[4], C. Schaerf[3], R.M. Sealock[5], H. Ströher[8], C.E. Thorn[1], S.T. Thornton[5], J. Tonnison[6,1], C.S. Whisnant[4], H. Zhang[7], X. Zhao[6]
*(The LEGS Collaboration)*

[1]Physics Department, Brookhaven National Laboratory, Upton, NY 11973
[2]INFN-Laboratori Natzionali di Frascati, Frascati, Italy
[3]Università di Roma "Tor Vergata" and INFN-Sezione di Roma2, Rome, Italy
[4]Department of Physics, University of South Carolina, Columbia, SC 29208
[5]Department of Physics, University of Virginia, Charlottesville, VA 22901
[6]Physics Department, Virginia Polytechnic Inst. & SU, Blacksburg, VA 24061
[7]Department of Physics, Ohio University, Athens, OH 45701
[8]II Physikalisches Institut, Universität Giessen, Giessen, Germany

## DISCLAIMER

BNL-64648



# The E2/M1 Ratio in $\Delta$ Photoproduction

A.M. Sandorfi[1], G. Blanpied[4], M. Blecher[6], A. Caracappa[1], C. Djalali[4], G. Giordano[2], K. Hicks[7], S. Hoblit[1,5], M. Khandaker[6,1], O.C. Kistner[1], A. Kuczewski[1], M. Lowry[1], M. Lucas[4], G. Matone[2], L. Miceli[1,4], B. Preedom[4], D. Rebreyend[4], C. Schaerf[3], R.M. Sealock[5], H. Ströher[8], C.E. Thorn[1], S.T. Thornton[5], J. Tonnison[6,1], C.S. Whisnant[4], H. Zhang[7], X. Zhao[6]
*(The LEGS Collaboration)*

[1]Physics Department, Brookhaven National Laboratory, Upton, NY 11973
[2]INFN-Laboratori Natzionali di Frascati, Frascati, Italy
[3]Università di Roma "Tor Vergata" and INFN-Sezione di Roma2, Rome, Italy
[4]Department of Physics, University of South Carolina, Columbia, SC 29208
[5]Department of Physics, University of Virginia, Charlottesville, VA 22901
[6]Physics Department, Virginia Polytechnic Inst. & SU, Blacksburg, VA 24061
[7]Department of Physics, Ohio University, Athens, OH 45701
[8]II Physikalisches Institut, Universität Giessen, Giessen, Germany

New high-precision measurements of $p(\vec{\gamma},\pi)$ and $p(\vec{\gamma},\gamma)$ cross sections and beam asymmetries have been combined with other polarization ratios in a simultaneous analysis of both reactions. Compton scattering has provided two important new constraints on the photo-pion amplitude. The E2/M1 mixing ratio for the $N \rightarrow \Delta$ transition extracted from this analysis is EMR = -3.0% ± 0.3 (stat+sys) ± 0.2 (model).

The properties of the transition from the nucleon to the $\Delta(1232)$ serve as a benchmark for models of nucleon structure. To first order, $N \rightarrow \Delta$ photo-excitation is dominated by a simple M1 quark spin-flip transition. At higher order, small L=2 components in the N and $\Delta$ wavefunctions allow this excitation to proceed via an electric quadrupole transition. Since Nucleon models differ greatly on the mechanisms used to generate these L=2 components, refs. [1–4], the ratio of E2/M1 transitions (EMR) provides a sensitive test for structure models.

The isospin $\tau = 3/2$ $\Delta$ decays with a 99.4% branch to $\pi$N final states and with a 0.6% $\gamma$N branch back to the nucleon ground state (Compton scattering). The most E2 sensitive observable is the beam asymmetry in $p(\vec{\gamma},\pi^{\circ})$, and the first precision measurements of this ratio were made at the Laser Electron Gamma Source (LEGS) [5]. These data, and preliminary asymmetries from the present experiment, have been used to fix the parameters in a number of models. In particular, the fitted $\gamma N\Delta$ couplings of the chiral Lagrangian model of Davidson, Mukhopadhyay and Wittman (DMW) [6] yielded an EMR of -2.7% [7], while Sato and Lee (SL) deduced -1.8% from their meson-exchange model [3].

There has been a recent measurement of the $p(\vec{\gamma},\pi)$ reaction in Mainz, and an EMR of -2.5% was extracted using a rather simplistic analysis of the $\pi^\circ$ channel [8], in which potential multipole ambiguities were ignored. In this paper we focus on minimizing ambiguities in the extraction of the E2 and M1 multipoles. We report an improved value for the EMR that is constrained by new measurements and two new observables, and demonstrate that the analysis applied to the Mainz data in [8] artificially inflated their EMR result by a factor of two.

At any energy, a minimum of 8 independent observables are necessary to specify the photo-pion amplitude [9]. Such complete information has never been available and previous analyses have relied almost exclusively on only four, the cross section and the three single polarization asymmetries, $\Sigma$ (linearly polarized beam), T (target) and P (recoil nucleon). The $\pi^\circ$ and $\pi^+$ channels have generally been measured separately, each with independent systematic errors which further complicates the situation. The $\tau = 3/2$ M1 and E2 components can still be extracted from a fit to a multipole expansion of the amplitude. But constraints from many observables are needed to avoid Donnachie's ambiguity [10] of higher partial wave strength appearing in lower partial waves, and vice versa. In the work reported here, $p(\vec{\gamma},\pi^\circ)$, $p(\vec{\gamma},\pi^+)$ and $p(\vec{\gamma},\gamma)$ cross sections and beam asymmetries have all been measured in a single experiment and a dispersion calculation of Compton scattering has been used to provide two new constraints on the photo-pion multipoles.

At LEGS, polarized tagged $\gamma$-ray beams between 209 and 333 MeV were produced by backscattering laser light from 2.6 GeV electrons at the National Synchrotron Light Source. Beams, with linear polarizations greater than 80% and known to $\pm 1\%$, were flipped between orthogonal states at random intervals between 150 and 450 seconds.

Both Compton scattering and $\pi^\circ$-production have a proton and at least one photon in their final states, and one goal of this experiment was the first complete separation of these two processes. This was accomplished by a large over-determination of kinematic parameters. The two reactions were distinguished by comparing their $\gamma$-ray and proton-recoil energies. High energy $\gamma$-rays were detected in a large NaI(Tl) crystal, while recoil protons were tracked through wire chambers and stopped in an array of plastic scintillators. A schematic of this arrangement and a spectrum showing the separation of the two channels is given in [11]. All detector efficiencies were determined directly from the data itself, an important advantage of this technique. For the Compton events, the solid angle was determined by the proton detectors.

For the $\pi^\circ$ channel the solid angle was a convolution of both the proton-recoil and the $\gamma$-ray detector acceptances. The uncertainty in the geometric solid angle was sampled by imposing successive proton acceptance and $\gamma$-ray energy cuts. The net $\pi^\circ$ cross sections were computed as the mean of these different analyses and their standard deviation was combined in quadrature with the statistical error ($\sim$ 1%) to yield a net *measurement* error.

Charged pions were detected in 6 NaI detectors, including the large crystal used for the Compton and $\pi^\circ$ channels, preceded by wire chambers. The recoil neutron was not detected. The beam energy and pion angle determined the $\pi^+$ energy. This resulted in spectra dominated by narrow peaks with tails due to nuclear reactions and $\pi \rightarrow \mu \rightarrow e$

decay. The high resolution of the NaI detectors was essential in determining $\pi^+$ efficiencies, which were simulated with GEANT [12] using GCALOR to model hadronic interactions [13]. Systematic effects were combined in quadrature with statistical errors ($\sim 1\%$) for a net *measurement* error.

In the vicinity of the $\Delta$ peak, the spin-averaged $\pi^\circ$, $\pi^+$, and Compton cross sections determined in this experiment are all consistently higher than earlier measurements from Bonn [14,17,18,21] while for energies lower than ~270 MeV substantial agreement is observed. Here we present results at 323 MeV and 265 MeV as examples of these energy regions. Angular distributions for p($\vec{\gamma},\pi^\circ$) and p($\vec{\gamma},\gamma$) are shown with their measurement errors as solid circles in figures 1 and 2, resp. In addition, all cross sections are locked together with a common systematic scale uncertainty, due to possible flux and target thickness variations, of 2%.

Recent Mainz cross sections for p($\gamma,\pi^\circ$) (open circles) [8], and older Bonn data [14], are both noticeably lower than our results and those of [15] near the $\Delta$ peak. Of previous $\pi^+$ cross section measurements, those from Tokyo [19] are closest to the present work.

In figure 2, two recent Compton measurements from Mainz at 90° and 75° are shown as open circles [22,23]. These data sets are in quite good agreement with the present work over our full energy range. As discussed in [11], earlier 90° Compton cross sections from Bonn [21] are about 28% too low in the vicinity of the $\Delta$ peak. Whatever their error, it is likely to be common to all angles measured with the same detector. The Bonn results are shown here, rescaled by 1.28 (open squares). The resulting angular distribution is in reasonable agreement with the present work.

To obtain a consistent description of these results we have performed an energy dependent analysis, expanding the $\pi$-production amplitude into electric and magnetic partial waves, $E^\tau_{\ell\pm}$ and $M^\tau_{\ell\pm}$ , with relative $\pi$N angular momentum $\ell$, and intermediate-state spin $j = \ell \pm \frac{1}{2}$ and isospin $\tau = \frac{1}{2}$ or $\frac{3}{2}$. A crucial factor in this type of analysis is the number of partial waves that are included. Here polarization data provide some guidance. Born terms contribute to quite high $\ell$, but are small in the $\pi^\circ$ channel. With only S and P waves, the $\pi^\circ$ polarization difference, $\frac{1}{2}(d\sigma_{\parallel}/d\Omega - d\sigma_{\perp}/d\Omega)$, is simply proportional to $\sin^2(\theta)$, while D waves introduce an additional $\cos(\theta)\sin^2(\theta)$ dependence. This polarization difference divided by $\sin^2(\theta)$ is shown in figure 3. D waves are clearly important in the region of the $\Delta$. Because the highest partial wave retained in a multipole expansion in inherently prone to ambiguities [10], we truncate our fit at F waves, while keeping the Born terms up to order $\ell = 19$.

The $(\gamma,\pi)$ multipoles were parameterized with a K-matrix-like unitarization,

$$A^\tau_{\ell\pm} = \left(A^\tau_B(E_\gamma) + \alpha_1\epsilon_\pi + \alpha_2\epsilon^2_\pi + \alpha_3\Theta_{2\pi}(E_\gamma - E^{2\pi}_\gamma)^2\right) \times \left(1 + iT^\ell_{\pi N}\right) + \beta \cdot T^\ell_{\pi N}. \qquad (1)$$

Here, $E_\gamma$ and $\epsilon_\pi$ are the beam and corresponding $\pi^+$ kinetic energies, and $A^\tau_B$ is the full pseudo-vector Born multipole, including $\rho$ and $\omega$ t-channel exchange [25]. The VPI[SM95] values are used for the $\pi$N scattering T-matrix elements [26]. Below $2\pi$ threshold, $E^{2\pi}_\gamma =$ 309 MeV, $T^\ell_{\pi N}$ reduces to $\sin(\delta_\ell)e^{i\delta_\ell}$, $\delta_\ell(E_\gamma)$ being the elastic $\pi$N phase shift, and $(1 + iT^\ell_{\pi N}) = \cos(\delta_\ell)e^{i\delta_\ell}$. Thus, eqn. 1 explicitly satisfies Watson's theorem [27] below $E^{2\pi}_\gamma$ and provides a consistent, albeit model-dependent, procedure for maintaining unitarity at higher energies. When a single s-channel resonance dominates a partial wave having only one open decay channel the last term in 1 exactly reduces to a Breit-Wigner energy

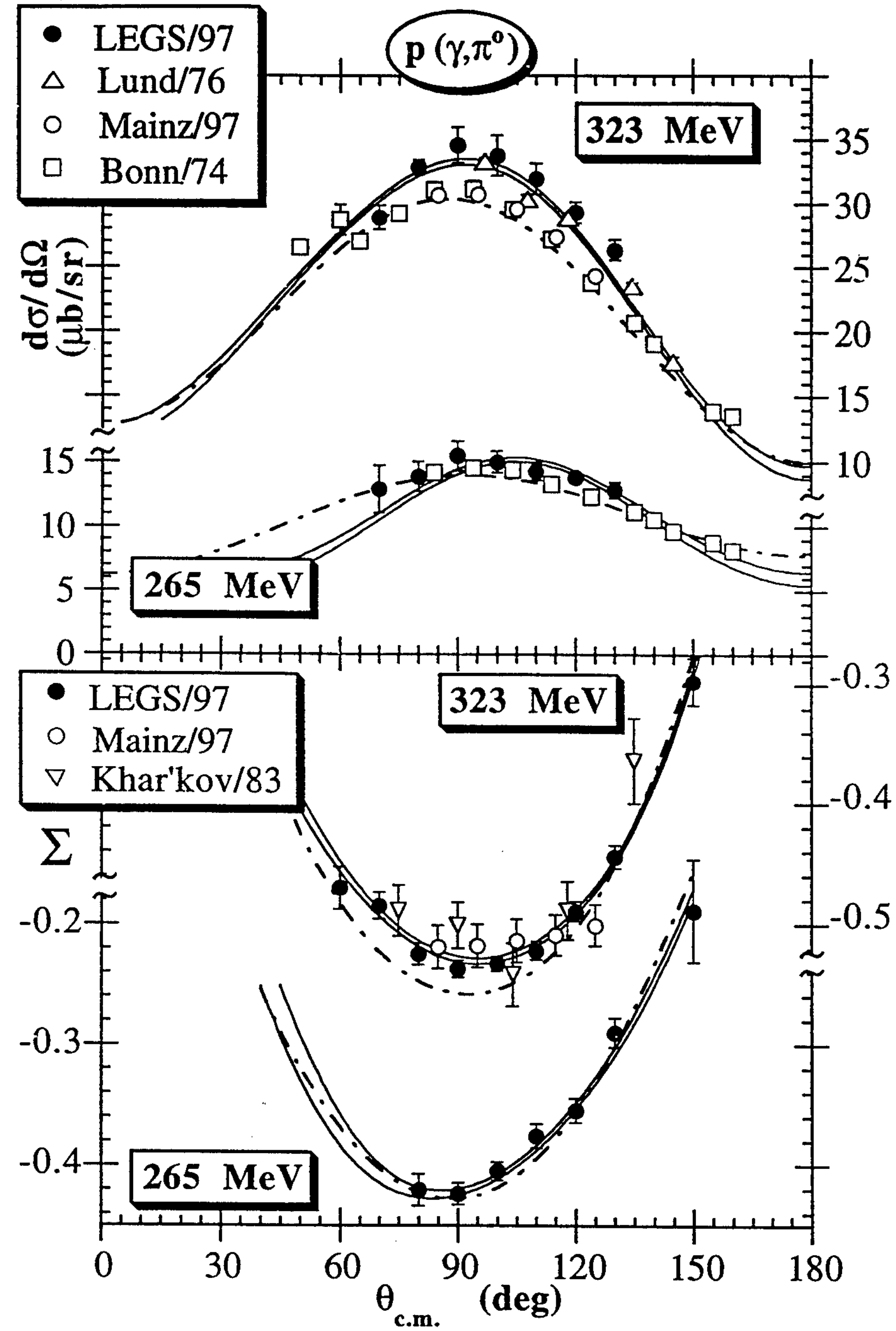


Figure 1. Cross sections (top row), and polarization asymmetries $\Sigma = (\sigma_{\parallel} - \sigma_{\perp})/(\sigma_{\parallel} + \sigma_{\perp})$ (bottom row), from the present work (solid points) for $p(\vec{\gamma}, \pi^{\circ})$ together with published data [8,14–16]. Results are shown for 265 MeV (323 MeV) beam energy with scales on the left (right) of each plot. Predictions from our multipole fit are shown with uncertainties as bands bounded by solid curves. Predictions from the VPI[SP97k] multipoles [26] are given by dash-dot curves.

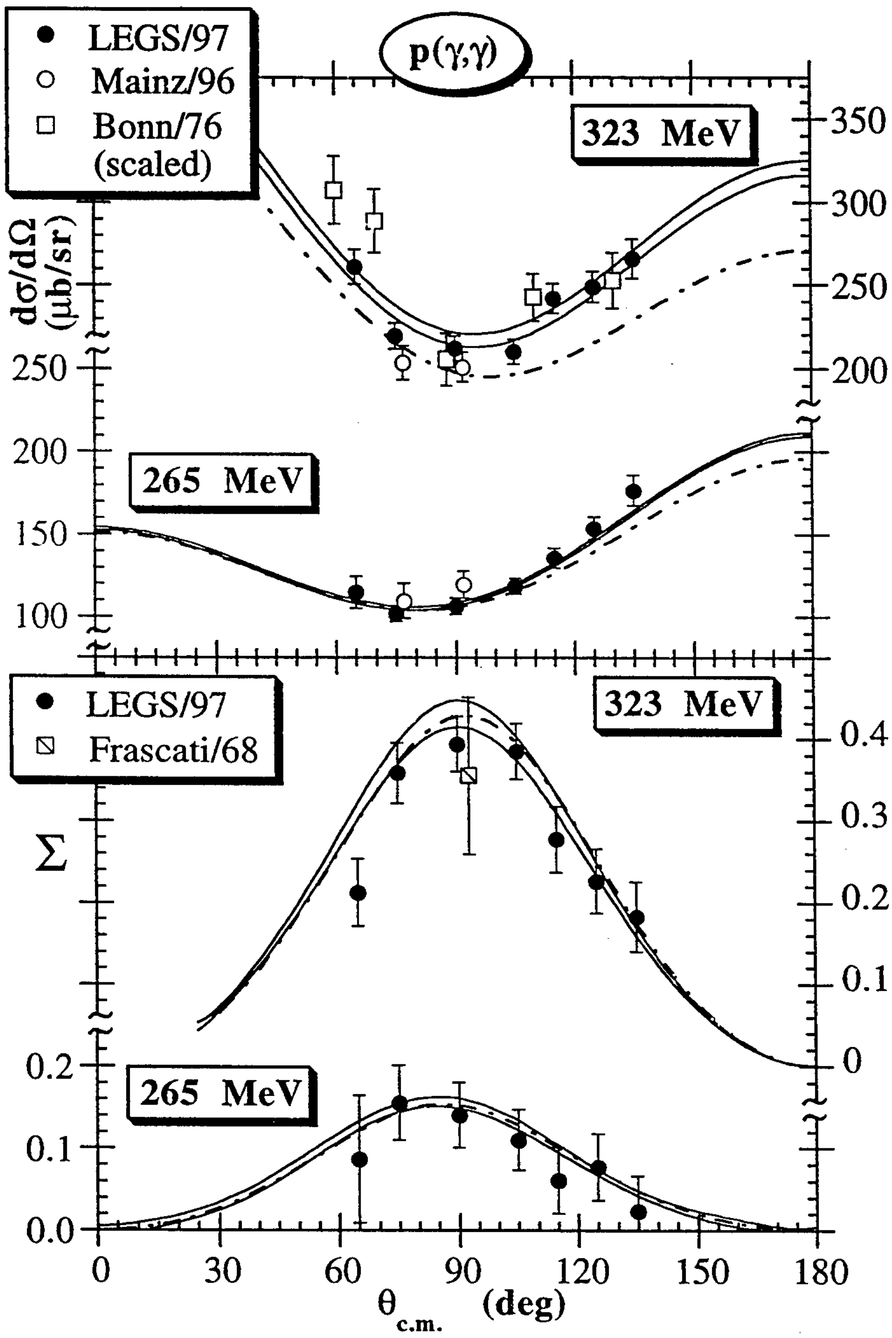


Figure 2. Cross sections (top row), and polarization asymmetries $\Sigma = (\sigma_{\parallel} - \sigma_{\perp})/(\sigma_{\parallel} + \sigma_{\perp})$ (bottom row), for $p(\vec{\gamma}, \gamma)$ together with published data [21–24]. Results are shown for 265 MeV (323 MeV) beam energy with scales on the left (right) of each plot. Predictions from our multipole fit are shown with uncertainties as bands bounded by solid curves. Predictions from the VPI[SP97k] multipoles [26] are given by dash-dot curves.

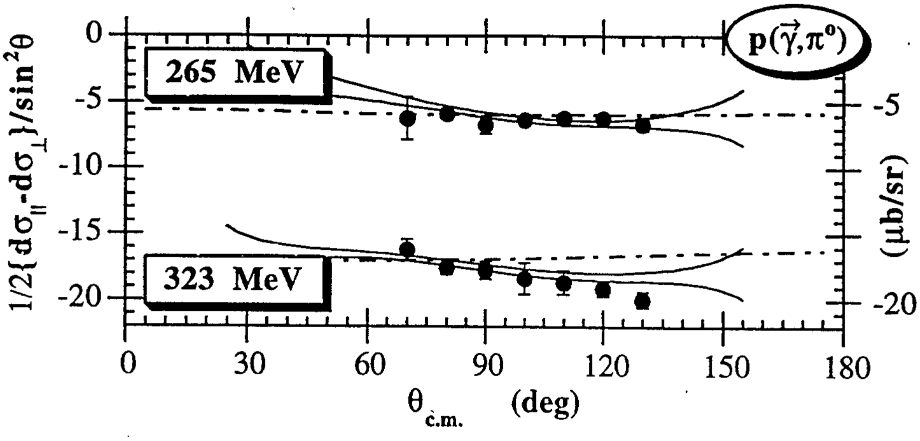


Figure 3. The linear polarization difference for p($\vec{\gamma}$, $\pi^\circ$) divided by $\sin^2\theta$ from the present work. Solid and dash-dot curves are as in fig. 1.

dependence. The $\beta$ term was fixed at zero for all multipoles except $M_{1+}^{3/2}$, $E_{1+}^{3/2}$, and $M_{1-}^{1/2}$, the first two describing M1 and E2 N $\rightarrow$ $P_{33}$ excitation and the latter allowing for a possible tail from the $P_{11}$ resonance. The other terms describe the non-resonant background, with the $\alpha_i$ included to account for non-Born contributions such as u-channel effects and pion rescattering. Each fitted multipole contains a term in $\alpha_1$, while the additional $\alpha_2$ term is used only in $E_{0+}^{1/2}$, $M_{1+}^{3/2}$ and $E_{1+}^{3/2}$. The $\alpha_3$ term containing the unit Heavyside step function $\Theta_{2\pi}$ (=1 for $E_\gamma > 309$ MeV) is used only in the $E_{0+}$ amplitudes to accommodate possible effects from S-wave $2\pi$ production.

Once the $(\gamma, \pi)$ multipoles are specified, the imaginary parts of the six Compton helicity amplitudes are completely determined by unitarity, and dispersion integrals can be used to calculate their real parts. Of these, only the two associated with helicity flip converge slowly. One is dominated by t-channel $\pi^\circ$ exchange (fixed by the $\pi^\circ$ lifetime), while the other can be recast into a sum rule for the nucleon polarizabilities. To predict the $(\gamma, \gamma)$ observables from the $(\gamma, \pi)$ amplitude we have implemented the computation of L'vov and co-workers [28]. The evaluation of the dispersion integrals requires $(\gamma, \pi)$ multipoles outside the range of the present work. For this we have used the VPI-SM95 solution up to 1.5 GeV [26], and estimates from Regge theory for higher energies [28]. Reasonable variations in these extrapolations do not result in significant changes within our energy range. The polarizabilities can also be extracted from this analysis, but they have only small effects on the N $\rightarrow$ $\Delta$ amplitudes and will be discussed in a separate publication.

We report here a summary of the results of a fit to the parameters of the $(\gamma, \pi)$ multipoles, minimizing $\chi^2$ for both predicted $(\gamma, \pi)$ and $(\gamma, \gamma)$ observables. In this fit we have used p($\vec{\gamma}$, $\pi^\circ$), p($\vec{\gamma}$, $\pi^+$) and p($\vec{\gamma}$, $\gamma$) cross sections only from the present experiment, since these are locked together with a small common scale uncertainty, and augmented our beam asymmetry data with other published polarization *ratios* (in which systematic errors tend to cancel). These include our earlier $\Sigma(\pi^\circ)$ data [5],{T($\pi^\circ$), T($\pi^+$)} data

Table 1
Dependence of the EMR on p($\gamma,\pi$) cross sections. Rows 1 and 3 summarize our multipole fit to p($\gamma,\pi$) and p($\gamma,\gamma$) using unpolarized p($\gamma,\pi$) results from this work in row 1, and substituting only the Bonn cross sections from [14,17] in row 3.

| Source | $\frac{d\sigma}{d\Omega}(\gamma,\pi)$ | EMR(%) | $\chi^2_{df}$ |
|---|---|---|---|
| $(\gamma,\pi)+(\gamma,\gamma)$ fit | LEGS | $-3.0\pm0.3$ | 1.63 |
| fit to DMW | LEGS | $-3.0+0.2/-0.3$ | |
| $(\gamma,\pi)+(\gamma,\gamma)$ fit | Bonn | $-1.3\pm0.2$ | 1.89 |
| Sato-Lee[3] | Bonn | $-1.8\pm0.9$ | |

from Bonn [29], {T($\pi^\circ$), P($\pi^\circ$), T($\pi^+$), P($\pi^+$)} data from Khar'kov [16,20], and the few beam-target asymmetry points {G($\pi^+$), H($\pi^+$)} from Khar'kov [30]. Systematic scale corrections were fitted following the procedure of ref. [31]. Although $2\pi$-production near threshold is quite small, the model dependences associated with maintaining unitarity at higher energies increase rapidly. To minimize these we have limited the fitting interval from 200 MeV to 350 MeV.

The predictions from the fitted $(\gamma,\pi)$ multipoles are shown in the figures as pairs of solid curves to indicate the corresponding uncertainty bands. The reduced $\chi^2$ for this analysis is $\chi^2_{df}=997/(644-34)=1.63$.

The EMR for N $\rightarrow\Delta$ is just the ratio of fitted $\beta$ coefficients in eqn. 1 for the $E^{3/2}_{1+}$ and $M^{3/2}_{1+}$ multipoles, -0.0296 $\pm$ 0.0021. (The quantity often compared to theoretical calculations is $R^{3/2}_{\rm EM}=\Im m(E^{3/2}_{1+})/\Im m(M^{3/2}_{1+})$ at the energy where $\delta_{P33}=90°$. From our fit, $R^{3/2}_{\rm EM}=-0.0294\pm0.0022$, which is essentially indistinguishable from our EMR since the inelasticities are very small and $(1+iT^{\ell}_{\pi N})\simeq\cos(\delta_\ell)e^{i\delta_\ell}=0$ at $\delta_{P33}=90°$.) The fitting errors reflects all statistical and systematic uncertainties. The full *unbiased estimate* of the uncertainty is $\sqrt{\chi^2}$ larger [32]. We have studied the variations that result from truncating the multipoles at D waves, using a different $\pi$N phase shift solution [33], allowing for differences in energy calibration between photoproduction and $\pi$N scattering, and varying the assumptions used to compute the Compton dispersion integrals [28]. The EMR is most sensitive to the multipole order and to the energy scale. Combining these *model* uncertainties in quadrature leads to our final results:

$$\text{EMR} = \text{-3.0\%} \pm 0.3\ (\text{stat+sys}) \pm 0.2\ (\text{model})\ .$$

Predictions from the recent VPI[SP97k] multipoles [26], which fit only the $(\gamma,\pi)$ reaction (including Bonn cross sections [14,17], the Mainz $\pi^\circ$ data [8], and our $\Sigma(\pi^\circ)$ data), are shown in the figures as dash-dot curves. For this solution, $R^{3/2}_{\rm EM}=-1.1\%$.

To investigate effects of lower $(\gamma,\pi)$ cross sections that dominate the VPI data base we have repeated our analysis, substituting Bonn values from [14,17] for our own $(\gamma,\pi)$ cross sections while keeping our Compton data and the same set of polarization asymmetries. The results are summarized in table I (row 3). The effect on the EMR is substantial and accounts for the lower VPI value.

In ref. [8], a fit to the recent Mainz $\pi^\circ$ cross section and $\Sigma(\pi^\circ)$ data, neglecting non-Born contributions beyond S and P waves, was used to extract an EMR of -2.5% $\pm$ 0.2 (stat)

± 0.2 (sys). The Mainz data agrees with Bonn cross sections [14] and LEGS $\Sigma(\pi^\circ)$ data, and thus should correspond to row 3 of table I. The factor of 2 difference between the (-1.3 ± 0.2)% value of row 3 and their reported result reflects ambiguities in their attempt to constrain the pion amplitude with only 2 observables. (In fact, the same criticism applies to the result of [7] in which DMW parameters were fitted to only our earlier $\Sigma(\pi^\circ)$ data and the Bonn cross sections.)

Various theoretical techniques have been used to separate the N $\rightarrow$ $\Delta$ component. Our result can be directly compared with models, such as DMW[6] and SL[3], that report ratios of $\gamma N \Delta$ couplings deduced with a K-matrix type unitarization equivalent to eqn. 1. We have refit the DMW parameters to our multipoles, with the result EMR = -3.0% +0.2/-0.3. This, and the result of SL who fitted their parameters to the Bonn cross sections and our $\{\Sigma(\pi^\circ), \Sigma(\pi^+)\}$ data, are listed in table I. The EMR values from these models are consistent with the set of $(\gamma, \pi)$ cross sections that were used to fix their parameters.

To summarize recent data and analyses, there are two new sets of measurements of $p(\gamma,\pi)$ and $p(\gamma,\gamma)$, the Mainz experiments reported in [8,22,23] and the LEGS experiment reported here and in [11]. While Compton cross sections measured in the two labs agree, $p(\gamma,\pi)$ cross sections do not. The EMR value quoted in [8] appears to agree with that of the present work, but this is purely accidental since their fitting procedure does not properly constrain the $p(\gamma,\pi)$ amplitude. A consistent analysis applied to both groups of data yields EMR values different by more than a factor of 2. The source of this difference is the $p(\gamma,\pi)$ cross section scale, and the advantage of the LEGS data lies in the fact that both $p(\gamma,\pi)$ and $p(\gamma,\gamma)$ channels are locked together with a small common systematic scale uncertainty.

LEGS is supported by the U.S. Dept. of Energy under Contract No. DE-AC02-76-CH00016, by the Istituto Nazionale di Fisica Nucleare, Italy, and by the U.S. Nat. Science Foundation. We wish to thank Mr. Frank Lincoln for his tireless help during these measurements. We are indebted to Drs. Anatoly L'vov and Shin-nan Yang for the use of their codes and many patient interactions. We are also grateful for useful discussions with Drs. G. Anton, F. Iachello, A. Nathan, and T.-S.H. Lee.

## REFERENCES

1. A. Wirzba and W. Weise, Phys. Lett. **B188**, 6 (1987).
2. R. Bijker, F. Iachello and A. Leviatan, Ann. Phys. **236**, 69 (1994).
3. T. Sato and T.-S.H. Lee, Phys. Rev. **C54**, 2660 (1996).
4. A.J. Buchmann, *et al.*, Phys. Rev. **C55**, 448 (1997).
5. LEGS Collaboration, G. Blanpied *et al.*, Phys. Rev. Lett. **69**, 1880 (1992).
6. R. Davidson, N. Mukhopadhyay and R. Wittman, Phys. Rev. **D43**, 71 (1991).
7. M. Khandaker and A.M. Sandorfi, Phys. Rev. **D51**, 3966 (1995).
8. R. Beck *et al.*, Phys. Rev. Lett. **78**, 606, (1997); H.-P. Krahn, thesis, U. Mainz (1996).
9. W. Chiang and F. Tabakin, Phys. Rev. **C55**, 2054 (1997).
10. A. Donnachie, Rep. Prog. Phys. **36**, 695 (1973).
11. LEGS Collaboration, G. Blanpied *et al.*, Phys. Rev. Lett. **76**, 1023 (1996).
12. GEANT 3.2.1, CERN Library W5013, CERN (1993).

13. *GCALOR*, C. Zeitnitz and T.A. Gabriel, Nucl. Instr. Meth. **A349**, 106 (1994).
14. H. Genzel *et al.*, Z. Physik **268**, 43 (1974).
15. P. Dougan*et al.*, Z. Physik **A276**, 155 (1976).
16. A. Belyaev *et al.*, Nucl. Phys. **B213**, 201 (1983).
17. G. Fischer *et al.*, Z. Physik **253**, 38 (1972).
18. K. Büchler *et al.*, Nucl. Phys. **A570**, 580, (1994).
19. T. Fujii *et al.*, Nucl. Phys. **B120**, 395 (1977).
20. V.A. Get'man *et al.*, Nucl. Phys. **B188**, 397 (1981).
21. H. Genzel *et al.*, Z. Physik **A279**, 399 (1976).
22. C. Molinari *et al.*, Phys. Lett. **B371**, 181 (1996).
23. J. Peise *et al.*, Phys. Lett. **B384**, 37 (1996); J. Ahrens, priv. comm.
24. G. Barbiellini *et al.*, Phys. Rev. **174**, 1665 (1968).
25. Shin-nan Yang, J. Phys. G11, L205 (1985); priv. comm.
26. *SAID*, telnet vtinte.phys.vt.edu; R. Arndt, I. Strakovsky and R. Workman, Phys. Rev. **C53**, 430 (1996).
27. K. Watson, Phys. Rev. **95**, 228, (1954).
28. A. L'vov *et al.*, Phys. Rev. **C55**, 359 (1997).
29. H. Dutz *et al.*, Nucl. Phys. **A601**, 319, (1996); Gisela Anton, priv. comm.
30. A.A. Belyaev *et al.*, Sov. J. Nucl. Phys. **40**, 83 (1984); *ibid*, **43**, 947 (1986).
31. G. D'Agostini, Nucl. Inst. Meth. **A346**, 306 (1994).
32. J.R. Wolberg, *"Prediction Analysis"*, Van Nostrand Co., NY, p. 54-66 (1967).
33. G. Höhler *et al., Handbook Pi-N Scattering*, Phys. Data **12**-1, Karlsruhe (1979).

M98000315

Report Number (14) BNL--64648
CONF-9705226--

Publ. Date (11) 199708
Sponsor Code (18) DOE/ER, XF
UC Category (19) UC-414, DOE/ER

DOE